

Accretion, jets and winds: High-energy emission from young stellar objects Promotionspreis lecture 2010

H. M. Günther^{1,*}

Harvard-Smithsonian Center for Astrophysics, 60 Garden Street, Cambridge, MA 02138, USA

Received 2011, accepted 2011

Published online later

Key words circumstellar matter – ISM: jets and outflows – stars: winds, outflows – T Tauri stars – X-rays: stars

This article summarizes the processes of high-energy emission in young stellar objects. Stars of spectral type A and B are called Herbig Ae/Be (HAeBe) stars in this stage, all later spectral types are termed classical T Tauri stars (CTTS). Both types are studied by high-resolution X-ray and UV spectroscopy and modeling. Three mechanisms contribute to the high-energy emission from CTTS: 1) CTTS have active coronae similar to main-sequence stars, 2) the accreted material passes through an accretion shock at the stellar surface, which heats it to a few MK, and 3) some CTTS drive powerful outflows. Shocks within these jets can heat the plasma to X-ray emitting temperatures. Coronae are already well characterized in the literature; for the latter two scenarios models are shown. The magnetic field suppresses motion perpendicular to the field lines in the accretion shock, thus justifying a 1D geometry. The radiative loss is calculated as optically thin emission. A mixture of shocked and coronal gas is fitted to X-ray observations of accreting CTTS. Specifically, the model explains the peculiar line-ratios in the He-like triplets of Ne IX and O VII. All stars require only small mass accretion rates to power the X-ray emission. In contrast, the HAeBe HD 163296 has line ratios similar to coronal sources, indicating that neither a high density nor a strong UV-field is present in the region of the X-ray emission. This could be caused by a shock in its jet. Similar emission is found in the deeply absorbed CTTS DG Tau. Shock velocities between 400 and 500 km s⁻¹ are required to explain the observed spectrum.

© 0000 WILEY-VCH Verlag GmbH & Co. KGaA, Weinheim

1 Introduction

Stars and planetary systems form by gravitational collapse of large molecular clouds. Mass infall leads to the formation of a proto-star, which is deeply embedded in an envelope of gas and dust. Due to the conservation of angular momentum matter from this envelope does not accrete directly onto the central star, but forms a proto-stellar disk around it. The envelope depletes and the central star becomes visible as stellar evolution proceeds. In this stage the stars are called classical T Tauri stars (CTTS), if they are of low-mass ($< 3M_{\odot}$, spectral type F or later) and Herbig Ae/Be stars (HAeBe), if they are of spectral type A or B. CTTS are cool stars with a convective photosphere, thus they generate magnetic fields in solar-like $\alpha - \Omega$ dynamos. Their field lines can reach out a few stellar radii and couple to the disk at the co-rotation radius, because the energetic radiation from the central star ionizes the upper layers of the disk. Thus, the accreting matter is forced to follow the magnetic field lines (Bertout et al. 1988; Koenigl 1991; Shu et al. 1994; Uchida & Shibata 1984). It is accelerated along the accretion funnel and hits the stellar surface at free fall velocity, so a strong shock develops. This magnetically-funneled accretion scenario explains the wide and unusual

emission line profiles observed in CTTS for H α and other Balmer lines (Muzerolle et al. 1998a,b). In fact, CTTS are often defined as young, low-mass stars with an H α equivalent width (EW) $> 10 \text{ \AA}$. Once the disk mass drops and the accretion ceases, the width of the H α line decreases and the stars are classified as weak-line T Tauri stars (WTTS). Eventually, the disk mass is completely absorbed in planets, accreted by the star or driven out of the system by stellar winds and photoevaporation, although transitional disks can exist in WTTS for some time (Padgett et al. 2006).

A wide range of observational evidence supports the magnetically-funneled accretion scenario for CTTS. Eisner et al. (2006) resolved the inner hole in the disk of TW Hya, the closest CTTS, with radio-interferometry. The accretion funnels are not resolved, but there is a very good agreement between observed and modeled line profiles for H α and other hydrogen emission lines, where emission from infalling material causes the blue-shifted wings of those lines (Fang et al. 2009; Muzerolle et al. 1998a,b). The energy from the accretion shock heats an area of the surrounding photosphere of the star to temperatures of the order of 20 000 K. In turn, this emits a hot black-body continuum, which veils the photospheric emission lines (Calvet & Gullbring 1998; Gullbring et al. 2000). The strength of the veiling in the UV and the optical wavelength range is one measure of the accretion rate. Some CTTS with fast rotation have been Doppler-imaged and hot spots on the surface can be seen

* Corresponding author: e-mail: hguenther@cfa.harvard.edu

(Strassmeier et al. 2005; Unruh et al. 1998). Zeeman-Doppler imaging reveals that the Ca infrared triplet originates in a region of strong magnetic fields, which, in the magnetically funneled accretion model, are the footpoints of the accretion funnels (Donati et al. 2007, 2008).

CTTS and WTTS are also copious emitters of X-rays and UV radiation; Feigelson & Montmerle (1999) review the knowledge before X-ray grating spectroscopy with *Chandra* and *XMM-Newton*. In this article I will discuss coronal activity, which is common to both CTTS and WTTS (section 2.1) and then summarize some observational characteristics in X-ray and UV spectroscopy, which set CTTS apart from main-sequence (MS) stars (section 2.2) to discuss accretion (section 2.3), winds (section 2.4) and stellar jets (section 2.5) in the following. Section 3 compares the properties of CTTS with HAEs. I end with a short summary in section 4.

2 Classical T Tauri Stars

X-ray emission from T Tauri stars (TTS) was discovered with the *Einstein* satellite (Feigelson & Decampli 1981). Starting with *ROSAT*, X-ray surveys were used as a tool to identify young stars in star forming regions, e.g. in the Taurus molecular cloud (Neuhäuser et al. 1995), the Chameleon star forming region (Alcala et al. 1995) and the Orion star forming cluster (Alcala et al. 1996), because young stars have a high level of X-ray activity. This continues today, mostly with *Chandra* because of its high imaging quality. One especially successful example is the Chandra Orion Ultradeep Project (COUP) with an exposure time of nearly 800 ks (Getman et al. 2005). However, the spectral information from these surveys remains poor by today's standards. Only the closest and brightest CTTS can be observed with high-resolution X-ray grating spectroscopy in a reasonable exposure time.

2.1 Coronal activity

For a long time the X-ray emission of CTTS was thought of as a scaled-up version of solar activity, because surveys of star forming regions show variability with a fast rise phase and a longer exponential decay in all types of TTS. CTTS and WTTS essentially share the same variability characteristics such as flare duration or the distribution of the flare luminosity, indicating that the same mechanism is responsible for the X-ray emission (e.g. Getman et al. 2008a,b; Stelzer et al. 2007). The majority of flares is small, and as their energy increases, occurrence becomes rarer. In general, the number of flares dN in the energy interval dE follows a power-law with $dN/dE \propto E^{-\alpha}$. The value of the exponent α in, e.g., the Taurus molecular cloud is 2.5 ± 0.5 (Stelzer et al. 2007), compatible with the solar value within the errors. This supports the idea that the majority of the X-ray emission on CTTS is coronal, just as the emission in WTTS or stars on the MS (see Güdel & Nazé 2009, for a review of stellar X-ray emission).

However, WTTS are on average twice as bright as CTTS (Preibisch et al. 2005; Stelzer & Neuhäuser 2001; Telleschi et al. 2007a), so there must be some difference in the X-ray generation.

2.2 Observational peculiarities

The following two subsections describe spectral properties, discovered in high-resolution X-ray spectra, which set CTTS apart from WTTS or MS stars.

2.2.1 He-like triplets

X-ray grating spectra show the He-like ions of C, O, Ne, Mg and Si. These ions emit a triplet of lines, which consists of a resonance (r), an intercombination (i), and a forbidden line (f) (Gabriel & Jordan 1969; Porquet et al. 2001). The flux ratios of those lines are temperature and density-sensitive. The R - and G -ratios ($R = f/i$ and $G = (f+i)/r$) are commonly used to describe the triplet; for high electron densities n_e or strong UV photon fields the R -ratio falls below its low-density limit, because electrons are collisionally or radiatively excited from the upper level of the f to the i line, but the UV field of late-type CTTS is too weak to influence the R -ratio. The G -ratio is a temperature diagnostic of the emitting plasma.

TW Hya was the first CTTS to be observed by *Chandra*/HETGS (for 50 ks). It showed an exceptional line ratio in the He-like triplets of O VII and Ne IX, which Kastner et al. (2002) interpret as a signature of high density. TW Hya has since been observed for 30 ks with *XMM-Newton* (Stelzer & Schmitt 2004), 120 ks with *Chandra*/LETGS (Raassen 2009) and for 500 ks again with *Chandra*/HETGS (Brickhouse et al. 2010). Together, this makes TW Hya one of the targets with the longest exposure times in the history of X-ray spectroscopy. Other CTTS were observed with grating spectroscopy, too: BP Tau (Schmitt et al. 2005), V4046 Sgr (Günther et al. 2006), RU Lup (Robrade & Schmitt 2007), MP Mus (Argiroffi et al. 2007) and Hen 3-600 (Huenemoerder et al. 2007) and they all show the same indication for high-densities that were first seen in TW Hya. Figures 1 and 5 (middle and right column) show examples for the He-like triplets in CTTS. TW Hya has the most extreme f/i ratio observed so far, but also more typical CTTS like V4046 Sgr differ markedly from the line ratio found in typical WTTS such as TWA 4 (Kastner et al. 2004) and TWA 5 (Argiroffi et al. 2005) and MS stars (Ness et al. 2004), which are compatible with the low-density limit of the f/i line ratio according to the CHIANTI 5.1 database (Dere et al. 1998; Landi et al. 2006).

There are exceptions to the high-densities in CTTS – in the more massive, eponymous T Tau itself the O VII triplet is consistent with the coronal limit (Güdel et al. 2007).

The O VII triplet is free of blends and its R -ratio is sensitive to densities of $10^{11} - 10^{12} \text{ cm}^{-3}$, but *Chandra*/ACIS data has a very low effective area at this wavelength. The Ne IX triplet is often blended with iron lines, particularly

Fe XIX and Fe XX. Strong sources provide sufficient signal in *Chandra*/HEG, where most of these blends are resolved, but for lower fluxes or observations with *XMM-Newton* these blends are difficult to remove, if the temperature structure is not very well known. Fortunately, most CTTS show an enhanced Ne abundance and a reduced Fe abundance, alleviating this problem to some extent (section 2.3).

The third interesting triplet is the Mg XI He-like triplet with lines at 9.17 Å, 9.23 Å and 9.31 Å. It can be blended by the higher members of the Ne X Lyman series. This problem is somewhat more serious in CTTS than in other objects, because of the enhanced Ne abundance often found in CTTS. For a few active MS stars Testa et al. (2004) extrapolated the strength of the higher order Ne X lines from the lower ones, which can be easily measured. They then fit the Mg XI triplet, taking the line blends into account. Brickhouse et al. (2010) analyzed their *Chandra*/HETGS observations and found that the blending is not important in this case.

For densities $< 10^{15} \text{ cm}^{-3}$ the collision time is much longer than the radiative decay time in the Lyman series, thus all excited states decay radiatively and the relative strength of the unabsorbed Ne X lines depends only on the temperature and the collision strength. I calculated the Lyman series up to Ly ϵ for a grid of temperatures with the CHIANTI 5.1 code (Dere et al. 1998; Landi et al. 2006) and extrapolated that series with a geometric function. In the observed spectra I fit as many members of the Lyman series as possible with the CORA tool (Ness & Wichmann 2002), which employs a maximum likelihood method, using a modified Lorentzian line profile with $\beta = 2.5$ and keeping the line width fixed at the instrumental width of 0.02 Å for the *Chandra*/MEG. The fits to the Mg XI triplet again use CORA. Here, the maximum likelihood is calculated for the sum of the extrapolated Ne X lines, Mg XI triplet and a constant, which represents a combination of background, continuum emission and unresolved lines. The likelihood is minimized with Powell's method by adjusting the individual flux of the triplet members, the constant and a wavelength offset. Both CTTS with archival *Chandra*/HETGS observations, TW Hya and V4046 Sgr, have very low fitted absorbing column densities for the accretion shock in the global fit (see section 2.3.2 and 2.3.3), thus the differential transmission between 9.1 Å and 12.13 Å is negligible. Table 1 gives the line fluxes found and figure 1 shows the fit. The constant is the strongest contributor to the total flux. Some of the Ne lines are clearly overpredicted, e.g. at 9.36 Å for TW Hya, others match the observations within the (large) Poisson errors. In any case, the Mg XI lines are not significantly blended by the Ne Lyman series. For TW Hya, this confirms the finding of Brickhouse et al. (2010).

The low-density limit of the f/i ratio for Mg XI is 2.5 for densities $< 10^{12} \text{ cm}^{-3}$; the ratio drops below 0.2 for densities $> 10^{14} \text{ cm}^{-3}$. Given the large statistical error on the line fluxes, neither the high-density nor the low-density limit can be excluded for TW Hya or V4046 Sgr, but at least

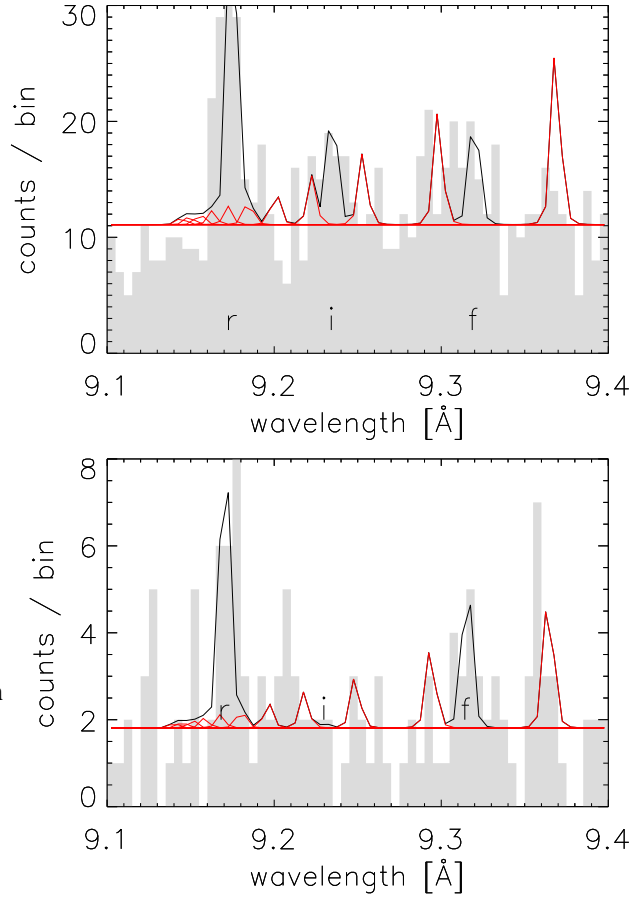


Fig. 1 Mg XI triplet of TW Hya (top) and V4046 Sgr (bottom). The gray histogram shows the observed counts, the lines show the best-fit model. Extrapolated lines of the Lyman series are plotted in red/gray (color in electronic version only).

for V4046 Sgr a low-density scenario is more likely as the i line is absent.

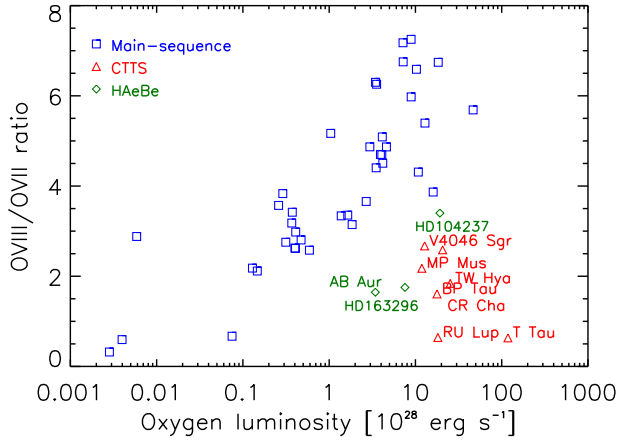
2.2.2 Ionization balance

To constrain the temperature and the origin of the plasma at low temperatures, which produces the anomalous R -ratios in the He-like triplets a line based method is preferable. Ideally, one would use the G -ratio of He-like triplets. Unfortunately, the temperature dependence of the G -ratio is weak and thus requires a high signal-to-noise ratio, which is only available for TW Hya. Brickhouse et al. (2010) use the higher order resonance lines of O VII for this purpose.

Alternatively, the balance of different ionization stages can be used as a temperature diagnostic. Robrade & Schmitt (2007) and Güdel & Telleschi (2007) constructed a diagram, which shows the ratio of the O VIII to the O VII lines and Günther & Schmitt (2009) added more stars (figure 2). The flux ratios in this diagram are based on unabsorbed luminosities, where the flux has been corrected for the extinction, which was found in a global fit, using the absorption

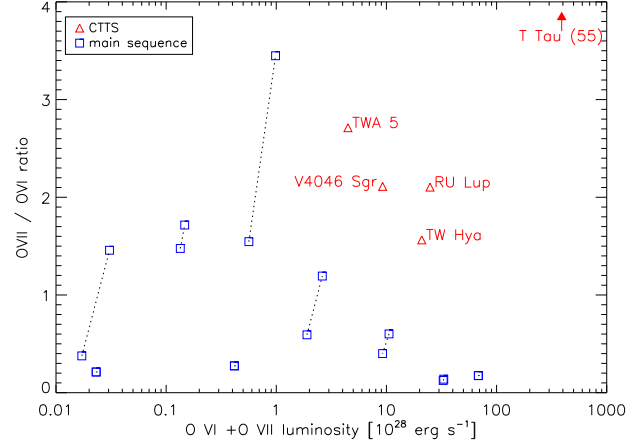
Table 1 Ne IX Ly series and Mg XI triplet fluxes (errors are 1σ confidence intervals)

| line | λ Å | TW Hya – Chandra | | V4046 Sgr – Chandra | |
|------------------|----------------|------------------|--------------------------------------|---------------------|--------------------------------------|
| | | cts | cts s ⁻¹ cm ⁻² | cts | cts s ⁻¹ cm ⁻² |
| Ne x Ly α | 12.13 | 1345 \pm 40 | (76. \pm 2.0) $\times 10^{-6}$ | 274 \pm 17 | (51. \pm 3.0) $\times 10^{-6}$ |
| Ne x Ly β | 10.24 | 247 \pm 17 | (8.3 \pm 0.6) $\times 10^{-6}$ | 57 \pm 8 | (5.6 \pm 0.6) $\times 10^{-6}$ |
| Ne x Ly γ | 9.71 | 73 \pm 10 | (2.4 \pm 0.3) $\times 10^{-6}$ | 25 \pm 6 | (2.4 \pm 0.6) $\times 10^{-6}$ |
| Ne x Ly δ | 9.48 | 62 \pm 11 | (1.5 \pm 0.3) $\times 10^{-6}$ | 25 \pm 8 | (2.0 \pm 0.7) $\times 10^{-6}$ |
| Mg XI r | 9.17 | 43. \pm 8.6 | (8.7 \pm 1.7) $\times 10^{-7}$ | 10. \pm 3.8 | (7.2 \pm 2.7) $\times 10^{-7}$ |
| Mg XI i | 9.23 | 16. \pm 6.4 | (3.3 \pm 1.3) $\times 10^{-7}$ | 0.1 \pm 1.7 | (0.07 \pm 1.2) $\times 10^{-7}$ |
| Mg XI f | 9.31 | 16. \pm 6.3 | (3.2 \pm 1.3) $\times 10^{-7}$ | 5.5 \pm 2.9 | (3.9 \pm 2.1) $\times 10^{-7}$ |

**Fig. 2** Flux ratio of O VIII Ly α and O VII He-like triplet, plotted over the sum of those emission lines. For comparison purposes MS stars from the Ness et al. (2004) sample are shown. Color in electronic version only.

cross-sections from Balucinska-Church & McCammon (1992). This step is necessary, because the extinction varies with wavelength, so different correction factors apply for O VIII at 18.97 Å and the O VII triplet around 21.8 Å. All CTTS are found at the bottom right of the diagram at comparatively high total luminosities. This is a selection bias, because X-ray grating spectroscopy can only be performed for the brightest CTTS in reasonable exposure times. The distance to the TW Hya association is about 57 pc, the next closest regions such as the Taurus-Auriga cloud or the ρ Oph cloud are located at a distance of 130 pc. In contrast, the MS sample from Ness et al. (2004) contains many closer stars and thus reaches down to lower luminosities. Still, the diagram shows an excess of O VII emission in CTTS compared to MS stars of similar luminosity. The peak emission temperature for the O VII lines is around 1-2 MK.

Following the same line of thought, the ratio of O VII and O VI emission will probe the cooler end of the plasma distribution. As no O VI emission lines are found in the X-ray range, they have to be taken from non-simultaneous observations with the *Far Ultraviolet Spectroscopic Explorer* (FUSE), which covers the wavelength range of the O VI doublet at 1032 and 1038 Å. The O VI fluxes for MS stars are taken from Redfield et al. (2002) and Dupree et al. (2005b), those for CTTS from Günther & Schmitt (2008). The ob-

**Fig. 3** Flux ratio of O VII He-like triplet to the O VI doublet at 1032 and 1038 Å, plotted over the sum of those emission lines. For comparison purposes MS stars are shown. If two X-ray observations are available in Ness et al. (2004), the figure shows two ratios calculated from those fluxes to give an estimate of variability. Color in electronic version only.

served FUSE fluxes are dereddened with the reddening law of Cardelli et al. (1989). The X-ray and UV observations are taken up to a few years apart, so the line ratios could be influenced by variability. To assess this figure 3 shows two flux ratios for those MS stars which have been observed multiple times in X-rays (Ness et al. 2004). Variability dominates over the formal measurement uncertainty, which is around 10% for most stars. Again, the CTTS are separated from MS stars in this diagram, although less significant than in figure 2. This time, they lie above the MS stars, indicating that they have extra O VII emission compared to MS stars with similar luminosity in the oxygen lines. So, CTTS are more luminous in O VII compared to both hotter (O VIII) and cooler (O VI) plasma than MS stars. Given that CTTS and WTTS seems to have very similar coronal emission, CTTS even appear to be hotter, it is unlikely, that this is caused by CTTS being underluminous in O VIII and O VI. A much better explanation for this excess of soft X-ray flux is an extra emission component at 1-2 MK (the formation temperature of the O VII He-like triplet) that is present in CTTS, but not in MS stars.

2.3 Accretion

One promising candidate for this extra emission is the accretion shock on the star. Here, an overview of accretion shock models is presented in section 2.3.1, then a sample of CTTS it described, where high resolution X-ray spectra indicate the presence of an accretion component (section 2.3.2). Section 2.3.3 shows model fits to this dataset. A comparison between our accretion shock model (Günther et al. 2007) and similar models in the literature is given in section 2.3.4.

2.3.1 Accretion models

The inner hole in the accretion disk is at least a few stellar radii wide, and thus the accretion impacts on the star close to free-fall velocity v_0 . For a star with mass M_* and radius R_* this is:

$$v_0 = \sqrt{\frac{2GM_*}{R_*}} = 600 \sqrt{\frac{M_*}{M_\odot}} \sqrt{\frac{R_\odot}{R_*}} \text{ km s}^{-1}. \quad (1)$$

Typically, CTTS have masses comparable to the Sun and radii between $R_* = 1.5 R_\odot$ and $R_* = 4 R_\odot$ (Muzerolle et al. 2003), because they have not yet finished their contraction. This gives infall velocities in the range $300\text{--}500 \text{ km s}^{-1}$. Not all kinetic energy is converted into thermal energy, because the total momentum needs to be conserved. In strong shocks the post-shock velocity v_1 is given by

$$v_1 = \frac{1}{4} v_0,$$

where v_0 is the pre-shock velocity. Particle number conservation then demands the following relation for the pre-shock particle number density n_0 and the post-shock number density n_1 :

$$n_1 = 4n_0.$$

The pre-shock pressure is completely dominated by the ram pressure of the infalling material, which drops dramatically across the shock front. In a quasi-equilibrium state, this is compensated by thermal pressure on the post-shock side and this leads to an expression for the post-shock temperature T_1 :

$$T_1 = \frac{3}{16} \frac{\mu m_H}{k} v_0^2,$$

where μ is the particle mass number, averaged over ions and electrons, and m_H is the mass of a hydrogen atom. k is the Boltzmann constant. For infall velocities close to the free-fall velocity this equation predicts extra emission at $1\text{--}2 \text{ MK}$. Strictly speaking, mostly the ions are heated in the strong shock, and it takes several mean-free path lengths to transfer heat to the electron gas. However, non-equilibrium ionization and temperature have a negligible effect on the final spectrum (Günther et al. 2007). After plasma passes through the accretion shock, it cools down via radiation. If the magnetic field of the accretion funnels is strong enough, all motion perpendicular to the field lines is suppressed and the problem can be simulated in 1D (sketch in figure 4).

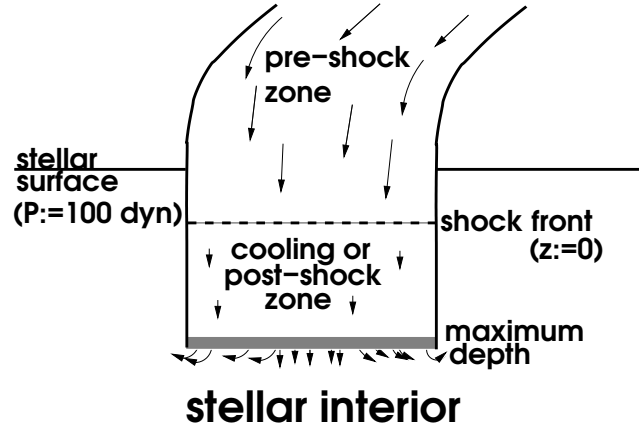


Fig. 4 Sketch of the accretion shock geometry. This sketch is not to scale. Matter falls in from the accretion streams and close to the stellar surface an accretion shock develops. In the post-shock zone the plasma cools via radiation. The stellar surface is arbitrarily represented at pressure $p = 100 \text{ dyn}$.

Calvet & Gullbring (1998) presented a grid of such models. They find that the radiation from the accretion shock heats the photosphere below the shock to about $20\,000 \text{ K}$. Their model fits the hydrogen continuum in the UV. Lamzin (1998) calculated the expected X-ray flux from the post-shock cooling zone. These simulations were updated by Günther et al. (2007) to resolve individual lines, especially in the He-like triplets. CTTS definitely show signs of coronal activity (section 2.1), so observed X-ray spectra have to be fitted with a combination of models which account for accretion and coronal contribution. Drake (2005) suggested that the shock might be buried in the photosphere, so that most of the X-ray radiation is absorbed by the surrounding photospheric gas. However, the fact that we observe high densities shows that at least some radiation escapes. While the photosphere would be a gray absorber, which affects all lines of the triplets simultaneously, emission from deeper layers of the post-shock cooling zone could experience line absorption. There are some hints to optical depth effects in the X-ray spectra (Argiroffo et al. 2009), but for most stars the G -ratios are close to the expected values. This excludes large optical depth effects, because the optical depth of the resonance line should be several orders of magnitude larger than in the forbidden or the intercombination line.

I calculated a grid of shock model with the code of Günther et al. (2007) for infall velocities between 300 km s^{-1} and 1000 km s^{-1} in steps of 100 km s^{-1} and infall densities between 10^{10} cm^{-3} and 10^{14} cm^{-3} in five logarithmic steps. The emission for all ions of C, N, O, Ne, Mg, Si, S and Fe is calculated separately from the continuum emission and the remaining elements, so that these abundances can be fit individually. However, large changes in the abundance would significantly alter the cooling function and thus the thermal structure of the shock. Simulations with different abundances found in the literature for CTTS were performed, and in this

range no significant change was observed. The model grid is provided as a table model. This table model is available at <http://www.hs.uni-hamburg.de/DE/Ins/Per/Guenther/wisfit.html>.

This basic shock interpretation has been extended by Brickhouse et al. (2010), who found a lower density and less absorption for O VII than for Ne IX in TW Hya, although the O VII triplet is formed at lower temperatures and therefore deeper in the post-shock cooling zone. They conclude, that most of the O VII emission does not originate in the accretion shock itself, but in plasma that has been heated by the shocked material. This situation can no longer be described in 1D. Simulations of the accretion shock region in more dimensions have been performed by Orlando et al. (2010). They show the flow to be well constrained for strong magnetic fields, but weaker fields cannot hold the plasma and mass flows sideways, thus changing the temperature and density profiles in the shock.

There is no a-priori reason to expect the shocks to be stable over time. Koldoba et al. (2008) and Sacco et al. (2008) both looked at this issue and predicted sub-second oscillations of the shock front, albeit at very different time scales, mostly due to the vastly different densities they assume in the shock. Observationally, this has not been found, neither in X-rays (Drake et al. 2009) nor in the optical response (Günther et al. 2010). This does not rule out fast oscillations of the shock front, it just requires the accretion along different field lines to oscillate independently with slightly different time constants.

2.3.2 Observations and fitting

Table 2 gives a list of X-ray observations of CTTS, where previous authors have found significant deviations from the low-density limit in the He-like triplets.

For observations split over several orbits, the day of the first exposure and the summed exposure time is given in the table. The *XMM-Newton* data was retrieved from the archive and processed with the standard *XMM-Newton* Science Analysis System (SAS) software, version 10.0 (Gabriel et al. 2004) with all standard selection criteria to filter out background contamination. *Chandra* data was retrieved from the archive and processed with CIAO 4.3 (Fruscione et al. 2006) to obtain CCD spectra; the grating spectra were taken directly from TGCat¹. Positive and negative first-order spectra were merged, then spectra from different orbits were combined, but HEG and MEG are kept separate. All CCD spectra were binned to 15 counts per bin, but grating data only to 5 counts per bin, because the density information in the triplets, which often contain only very few counts, would be destroyed by a coarser binning.

2.3.3 A sample of CTTS

For small count numbers a χ^2 statistic is no longer applicable, instead the fit was done using the C-statistic. Still,

¹ <http://tgcat.mit.edu>

the CCD spectra with their higher count rates tend to dominate the statistic. For *XMM-Newton* data only the MOS1 was fitted and for the *Chandra* spectra only the ACIS zeroth order of one of the available exposures. In this way, the cool shock component, which is mostly constrained by the information from the gratings is effectively fitted, otherwise the optimization would prefer small improvements in the coronal components at the prize of systematic deviations in the low energy region because the hot components cause higher CCD count rates. The C-statistic takes the proper Poisson uncertainties in bins with small count number into account, but it does not provide a goodness-of-fit.

X-ray spectra can be used to fit relative abundances of metals, but it is very difficult to obtain absolute abundances. Thus, the abundance of oxygen is fixed at solar (Grevesse & Sauval 1998) for all models in this section, i.e. all abundances are given relative to oxygen. The abundances of C, N, Ne, Mg, Si and Fe are fitted independently. The abundance of S is coupled to Fe, all other abundances are fixed at solar values. Because *Chandra*/ACIS has low effective areas at longer wavelengths, where the lines of C and N are observed, I fixed the abundance of those two elements at solar values for all *Chandra* data sets and, additionally, the absorbing column density for TW Hya in the *Chandra* data was fixed to the value found in the *XMM-Newton* observation.

Fits to the CTTS sample were obtained with XSPEC 12.6 (Arnaud 1996), fitting four model components: Three emission components (one shock model and two optically thin thermal APEC models, which represent the corona) and one cold photo-absorption component. Figure 5 shows the fitted low-resolution spectra (left panels) and also the fits to the He-like ions Ne IX (middle panels) and O VII (right panels). The results are summarized in table 3. The panels show the contribution of shock and corona independently. The corona is responsible for the hot emission, which cannot be explained by the accretion shock, because such high temperature would require infall velocities above the free-fall velocity. The He-like triplets are predominantly formed at lower temperatures in the accretion shock. This can be immediately seen from the strong *i* line. The corona is in the low density limit and thus its *f/i* ratio is high in contrast to the observations. Therefore, the *i* line has to be formed in the shock, which automatically requires the shock to contribute most of the emission in the *r* and *f* lines as well.

Table 3 only shows the statistical uncertainties for the fit, not any systematic model uncertainties. The plasma temperatures e.g. just represent the average plasma properties. The small statistical uncertainties on the temperature do not mean that the plasma temperature distribution is bimodal with very narrow peaks. Fits which prescribe e.g. polynomial emission measure distributions are also possible.

The mass accretion rate \dot{M} is related to the accretion spot size A , the infall velocity v_0 and the density n_0 as:

$$\dot{M} = \mu m_{\text{H}} n_0 v_0 A. \quad (2)$$

For most stars the signal in the He-like ions is relatively weak and the statistical error on the density is large. The er-

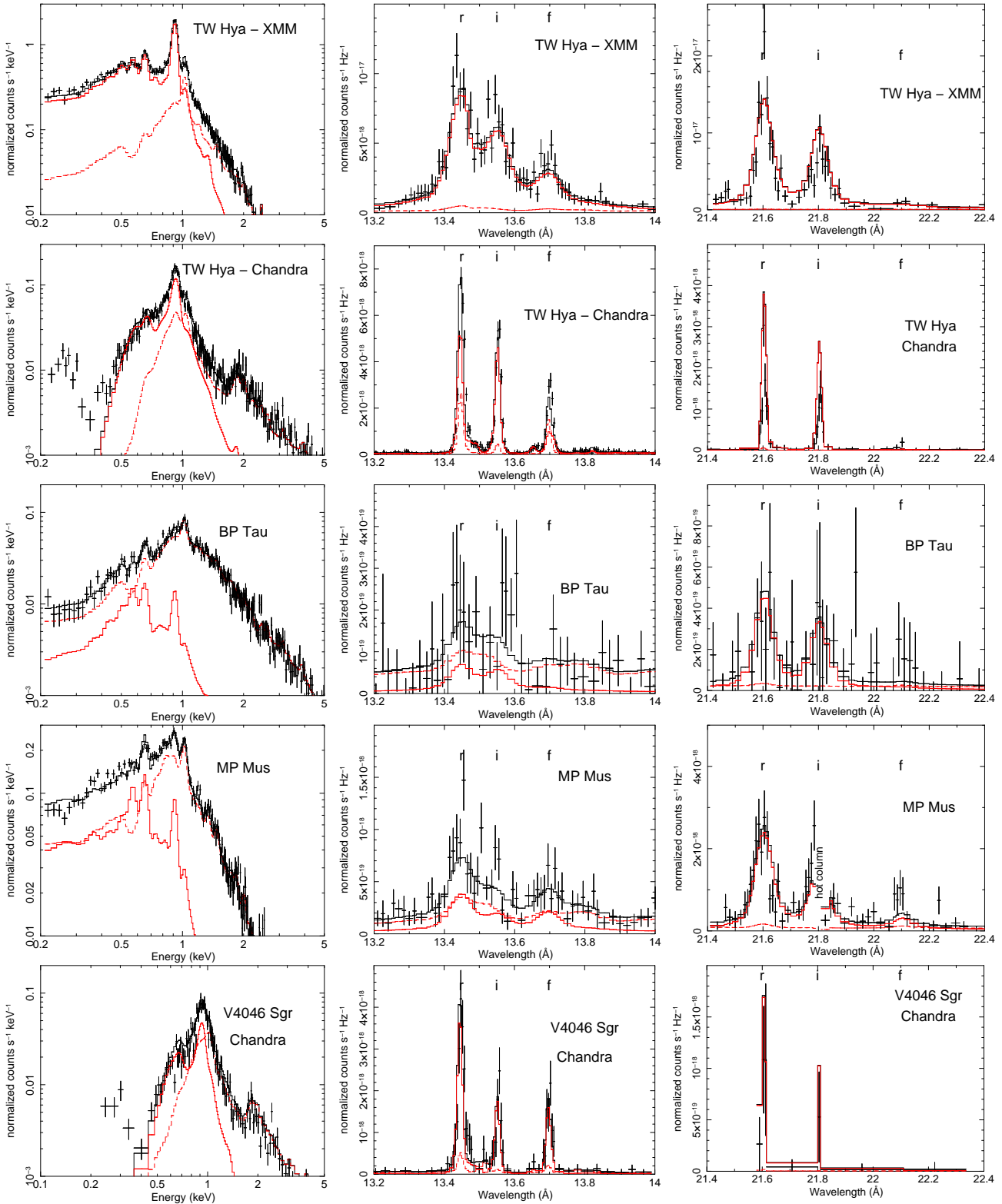


Fig. 5 Spectra of CTTS with fitted model overplotted. The panels show spectra in CCD resolution (left) and grating data for the Ne IX (middle) and O VII (right) He-like triplets. Best-fit models are overplotted, the contribution of corona (red/gray dashed) and shock (red/gray) is shown individually. In the He-like triplets most emission comes from the shock. The wavelength of the *r*, *i* and *f* line is labeled. The second and fifth row show *Chandra* data, which has narrower lines in the grating spectra, but little effective area at lower wavelength in the CCD spectra.

Table 2 Observations

| star | satellite | exp. time [ks] | obs date | ObsID |
|-----------|------------|-------------------|------------|------------------------|
| TW Hya | XMM-Newton | 30 | 2001-07-09 | 0112880201 |
| TW Hya | Chandra | 490 | 2007-02-15 | 7435, 7436, 7437, 7438 |
| BP Tau | XMM-Newton | 130 | 2004-08-15 | 0200370101 |
| MP Mus | XMM-Newton | 110 | 2006-08-19 | 0406030101 |
| V4046 Sgr | Chandra | 150 | 2006-08-06 | 5423, 6265 |

Table 3 Fit results (errors are statistical only and give 90% confidence intervals)

| | TW Hya <i>XMM-Newton</i> | TW Hya <i>Chandra</i> | BP Tau <i>XMM-Newton</i> | MP Mus <i>XMM-Newton</i> | V4046 Sgr <i>Chandra</i> |
|--|---------------------------------|--------------------------|---------------------------------|-----------------------------------|---------------------------------|
| absorbing column density | | | | | |
| $N_H [10^{20} \text{ cm}^{-2}]$ | $5.2^{+0.6}_{-0.4}$ | $=5.2$ | 14 ± 4 | 2 ± 1 | 6 ± 3 |
| abundances relative to O | | | | | |
| C | 1.5 ± 0.2 | $=1$ | $2.2^{+2.4}_{-1.7}$ | 1.4 ± 0.4 | $=1$ |
| N | 3.0 ± 0.3 | $=1$ | 2.2 ± 1.2 | 1.6 ± 0.4 | $=1$ |
| Ne | $7.6^{+3.2}_{-2.6}$ | 3.2 ± 0.2 | 1.7 ± 0.5 | 1.8 ± 0.2 | 3.5 ± 0.4 |
| Mg | 1.0 ± 0.3 | 0.36 ± 0.05 | 0.3 ± 0.3 | 0.8 ± 0.2 | 0.5 ± 0.1 |
| Si | 0.8 ± 0.3 | 0.5 ± 0.1 | 0.2 ± 0.2 | 0.6 ± 0.2 | 0.6 ± 0.1 |
| Fe | 0.9 ± 0.1 | 0.42 ± 0.03 | 0.2 ± 0.1 | 0.5 ± 0.1 | 0.46 ± 0.06 |
| coronal components | | | | | |
| $kT_1 [\text{keV}]$ | $0.69^{+0.04}_{-0.02}$ | 0.36 ± 0.01 | 0.7 ± 0.1 | 0.63 ± 0.03 | 0.73 ± 0.04 |
| $VE M_1 [10^{51} \text{ cm}^{-3}]$ | 7.2 ± 1.2 | 27 ± 2 | 43 ± 2 | 83 ± 15 | 28 ± 5 |
| $kT_2 [\text{keV}]$ | $1.7^{+0.2}_{-0.1}$ | 2.0 ± 0.05 | 2.2 ± 0.2 | 2.2 ± 0.1 | 2.2 ± 0.2 |
| $VE M_2 [10^{51} \text{ cm}^{-3}]$ | 19 ± 1.5 | 37 ± 1 | 100 ± 10 | 111 ± 5 | 38 ± 3 |
| shock properties | | | | | |
| $v_0 [\text{km s}^{-1}]$ | 500 ± 5 | 504 ± 3 | 440^{+70}_{-25} | 510 ± 10 | 500^{+10}_{-50} |
| $\log(n_0) [\text{cm}^{-3}]$ | 11.9^a | 13.0^a | 12.9^a | 11.1 ± 0.2 | 11.2^a |
| $A [\text{cm}^2]$ | 6.5×10^{19} | 4×10^{18} | 4×10^{20} | 4×10^{20} | 3×10^{20} |
| $\dot{M} [M_\odot \text{ yr}^{-1}]$ | 7×10^{-11} | 6×10^{-11} | 4×10^{-9} | 6×10^{-11} | 6×10^{-11} |
| X-ray mass accretion rates from literature | | | | | |
| $\dot{M} [M_\odot \text{ yr}^{-1}]$ | $2 \times 10^{-11} \text{ (1)}$ | | $9 \times 10^{-10} \text{ (2)}$ | $2 \times 10^{-11} \text{ (3)}$ | $3 \times 10^{-11} \text{ (4)}$ |
| $\dot{M} [M_\odot \text{ yr}^{-1}]$ | $2 \times 10^{-10} \text{ (5)}$ | | | $7.7 \times 10^{-11} \text{ (6)}$ | |

(a) The model grid uses density steps of 1 in log-space. Here, the interpolation error between two models is much larger than the statistical uncertainty. (1) Stelzer & Schmitt (2004); (2) Schmitt et al. (2005); (3) Argiroffi et al. (2007); (4) Günther & Schmitt (2007); (5) Günther et al. (2007); (6) Sacco et al. (2008)

ror in n_0 and A is then correlated such that a small accretion spot with a high density or a large accretion spot with a low density are both possible, if they have the same mass accretion rate and thus the same total luminosity. So, while n_0 and A are uncertain, \dot{M} is still a well-determined quantity. Fitted mass accretion rates are given in table 3.

The sample was selected to contain only stars with high densities. The prime example is TW Hya, where Kastner et al. (2002) observed 10^{13} cm^{-3} , Stelzer & Schmitt (2004) the same, Raassen (2009) 10^{12} cm^{-3} and Brickhouse et al. (2010) between $6 \times 10^{11} \text{ cm}^{-3}$ and $3 \times 10^{12} \text{ cm}^{-3}$ for O VII and Ne IX respectively. In BP Tau Schmitt et al. (2005) find $3 \times 10^{11} \text{ cm}^{-3}$, Günther et al. (2006) give $3 \times 10^{11} - 10^{12} \text{ cm}^{-3}$ for V4046 Sgr and Argiroffi et al. (2007) found $5 \times 10^{11} \text{ cm}^{-3}$ in MP Mus. This is largely consistent with the post-shock values expected from the pre-shock densities given in table 3.

If, however, the cool emission is formed only partly in a high-density accretion shock and partly in a low-density

corona, the f/i ratio in the He-like triplet can indicate medium densities. In this case, the \dot{M} is overestimated. One further problem of the model chosen in this paragraph shows up in TW Hya. Brickhouse et al. (2010) found that the accretion shock is less absorbed than the corona in TW Hya and the absorbing column density differs even between Ne IX and O VII. Also, Ne IX indicates a larger density than O VII, although it should be formed higher in the accretion shock. All this is not reproduced by the simple model used here and figure 5 shows that Ne IX is fitted very well for TW Hya, while O VII is overpredicted.

Unfortunately, TW Hya is the only CTTS with such a high signal-to-noise in the spectrum that these differences to the model can be seen. Similar shortcomings as in TW Hya might exist for the other CTTS but would be hidden in the noise. The best I can do to compare the mass accretion rates for several CTTS consistently is to fit all stars in the sample with a consistent model.

The table also shows, that the Ne abundances are enhanced in all CTTS, while the abundances of Fe, Si and Mg are reduced. Stelzer & Schmitt (2004) put forward the idea that Fe, Si and Mg condense on grains and settle, but the noble gases cannot and are accreted onto the star. However, Ne also has a higher first ionization potential and in all active stars the coronal abundance of those elements is enhanced (IFIP effect) (see the review by Güdel & Nazé 2009). Even for TW Hya the signal is not strong enough to determine the Ne abundance in the shock and the corona independently, so any one or both of the above scenarios might be important.

In most cases, the corona is described by one temperature component with $kT \approx 0.7$ keV and another with $kT \approx 2$ keV; the volume emission measures VEM of the corona vary over the sample. That is not surprising as several of the lightcurves contain strong flares which cause higher temperatures and higher emission measures for the duration of the flare.

The fitted values for the infall velocity in all stars are compatible with estimates for the free-fall velocity. The normalization of the shock models is proportional to the total mass flux, with is around $6 \times 10^{-11} M_{\odot} \text{ yr}^{-1}$ for TW Hya, MP Mus and V4046 Sgr. TW Hya and MP Mus are both relatively old CTTS, so a smaller mass accretion rate here is expected. The mass accretion rate of BP Tau is two orders of magnitude stronger.

2.3.4 Comparison of mass accretion rates

The shock models fitted in the previous section agree with other estimates in the literature, that are also based on X-ray spectra, within a factor of 2-4 (table 3). Some of those estimates are far simpler (Argiroffi et al. 2007; Schmitt et al. 2005; Stelzer & Schmitt 2004). They just use the fitted volume emission measure and density with a single value for the cooling function and some rough estimate for the depth of the post-shock cooling zone. Still, the results are comparable. In the case of TW Hya the mass accretion rates of both observations agree. Again, this shows that the fitting of the mass accretion rates is relatively robust, but the density should be determined from line fitting and not with a global fit on binned spectra.

However, all X-ray determined mass accretion rates are one or two orders of magnitude smaller than measurements obtained with the UV flux or the optical veiling (Curran et al. 2010). It is unknown what causes this effect. One possibility are inhomogeneous accretion spots. Either only a small part of the accretion stream impacts at free-fall velocity and the remaining mass accretes at a lower velocities or parts of the accretion spots are hidden by complete absorption. Although some hydrodynamical simulations of accretion streams show inhomogeneous impact velocities (Long et al. 2007; Romanova et al. 2004), it remains unclear which physical mechanism reduces the speed and where the corresponding gravitational energy is lost. Also, Argiroffi et al. (2009) find no resonant scattering in the O VII lines in TW Hya, thus is

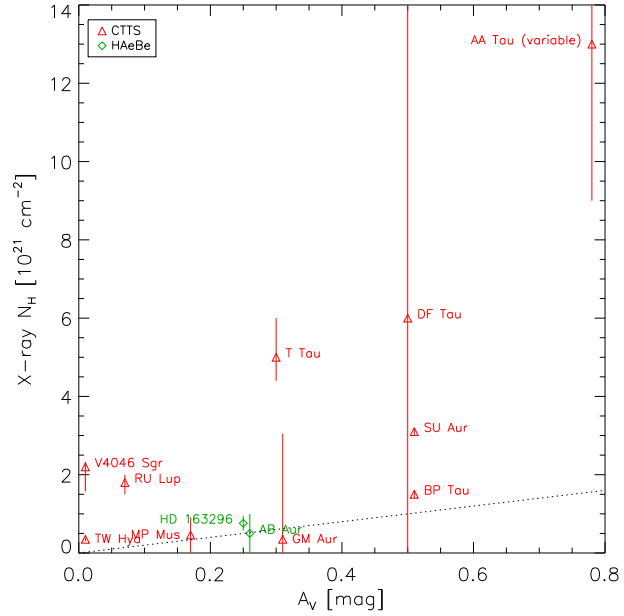


Fig. 6 Optical reddening and X-ray absorbing column density (with 90% confidence error bars). The dotted line shows the interstellar gas-to-dust ratio. DM Tau and GM Aur have *ROSAT*/PSPC spectra only, so the error bars are much larger.

seems unlikely that absorption can explain the small mass accretion rate found.

2.4 Winds

Many, if not all, CTTS have outflows (a review is given by Bally et al. 2007), but the physical driving mechanism is unknown. Theoretical models propose a variety of stellar winds (Kwan & Tademaru 1988; Matt & Pudritz 2005), X-winds (Shu et al. 1994) and disc winds (Anderson et al. 2005; Blandford & Payne 1982). Winds, which could be of stellar origin or come from the disk, are observed over a wide wavelength range from radio to the UV (e.g. Alencar & Basri 2000; Beristain et al. 2001; Dupree et al. 2005a; Edwards et al. 2006; Lamzin et al. 2004). Some CTTS also have highly collimated jets, which are discussed in more detail in section 2.5. The dynamics of the gas around CTTS are measured by UV spectroscopy with *HST*/*GHRs*, *HST*/*STIS* and *FUSE* (Ardila et al. 2002a,b; Herczeg et al. 2002, 2006, 2005). The best-studied CTTS is TW Hya, where Dupree et al. (2005a) fit the asymmetric line profile of the O VI 1032 Å line with a Gaussian with the centroid matching the stellar rest-frame. They explain the missing flux on the blue side of the line by a spherically-symmetric and smoothly-accelerated hot wind. However, Johns-Krull & Herczeg (2007) argue that this model is incompatible with *HST*/*STIS* observations, especially for the C IV 1550 Å doublet. The existence of a hot wind in TW Hya, therefore, remains an open issue. Günther & Schmitt (2008) extracted line profiles for all CTTS in the *FUSE* archive and find line centroids to be shifted between -170 km s^{-1}

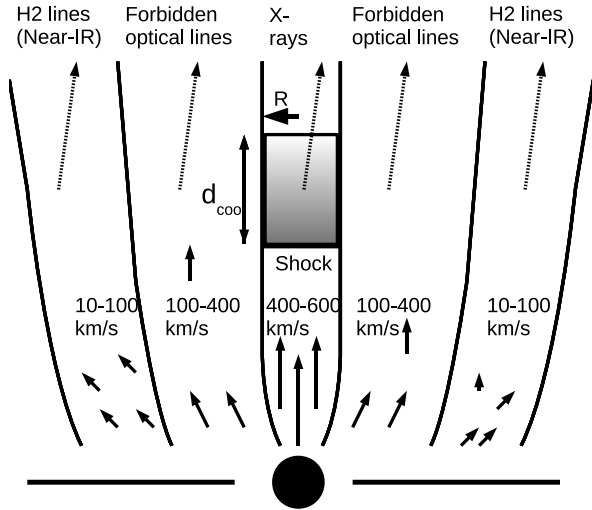


Fig. 7 Sketch of a cut through the outflow from a CTTS (not to scale). The inner components of the outflow are more collimated and faster and thus heat to higher temperatures when shocked.

and $+100 \text{ km s}^{-1}$. The blue-shifted emission is likely caused by shocks in outflows from the CTTS.

Figure 6 compares the gas column density as measured by X-rays with the optical reddening, which is mainly caused by dust (see Günther & Schmitt 2008, and references therein for data sources). The optical reddening is notoriously difficult to measure in accreting systems, but at least in some cases, notably V4046 Sgr, RU Lup and T Tau, the gas absorption is much higher than expected from an interstellar gas-to-dust ratio (Vuong et al. 2003) and the optical reddening. These are also the stars with blue-shifted UV emission. It is possible that the same outflows, which provide the UV emission lines also act as dust-depleted absorbers for the stellar light.

2.5 Jets

In addition to wide-angle winds CTTS can also drive highly collimated jets (Coffey et al. 2004; Güdel et al. 2005; Rodríguez et al. 1995), but DG Tau is the only CTTS where X-ray emission has been found from the jets. Other X-ray jets like HH 2 (Pravdo et al. 2001) or HH 154 (Bally et al. 2003; Favata et al. 2006, 2002) have younger and more embedded driving sources. Usually, the inner components of these jets are faster and denser (figure 7). Bacciotti et al. (2000) used the *HST* to resolve the jet of DG Tau in several long-slit observations. The emission of gas faster than 200 km s^{-1} is mostly confined to the inner slit, corresponding to a radius of 15 AU. The ratios of [O I], [N II] and [S II] give a lower limit on the gas density of 10^4 cm^{-3} . This component seems to be surrounded by slower moving gas with lower densities of the order $10^3 - 10^4 \text{ cm}^{-3}$. On larger scales an even cooler outflow, with an opening angle of 90° is seen

in molecular hydrogen (Takami et al. 2004). Lavalley et al. (1997) estimate a mass loss rate of $6.5 \cdot 10^{-6} M_\odot \text{ yr}^{-1}$ assuming shock heating in the gas. Hartigan et al. (1995) obtain $3 \cdot 10^{-7} M_\odot \text{ yr}^{-1}$. The kinematics of the gas can be calculated from line shifts and proper motion, accounting for the inclination of the jet to the plane of the sky. Optical and IR lines are blue-shifted up to deprojected velocities of 600 km s^{-1} (Bacciotti et al. 2000; Lavalley-Fouquet et al. 2000; Pyo et al. 2003) and the proper motion of the knots in the jets is $0''.28 \text{ yr}^{-1}$, which translates into a deprojected velocity of 300 km s^{-1} (Pyo et al. 2003).

In this context, the X-ray emission from the jet can be understood as shock-heated plasma from the densest and innermost component of the outflow (Günther et al. 2009). Only 10^{-3} of the total mass outflow is required to shock at the velocities observed in the fastest jet component to explain the observed X-ray spectra and emission measures. Given the density from the forbidden emission lines and the temperature for the X-ray spectrum the cooling length d_{cool} can be calculated with a model very similar to the accretion shock model. The total intensity determines the volume emission measure of the plasma and with the density and d_{cool} this yields the area of the shock. For DG Tau the estimated dimensions are only a few AU, if all X-ray emission is produced in a single shock (figure 7). Because of the small dimensions, a shock in the innermost component does not necessarily disturb the flow in the outer layers, which are resolved with the *HST*. So far, this model is compatible with all available observations.

3 Herbig Ae/Be stars

Herbig Ae/Be stars (HAeBes) are in a similar evolutionary state as CTTS, but they have spectral type A or B. Due to their higher mass their evolution progresses faster and typically they are younger than CTTS. Like CTTS HAeBes are surrounded by a disk and they actively accrete matter, but they are not expected to have an outer convective envelope, thus they should not generate magnetic fields and coronal activity. It is unclear if they can support magnetically funneled accretion. Zinnecker & Preibisch (1994) discovered X-ray emission from many HAeBes. More recent studies with the current generation of X-ray telescopes often identify the X-rays with a co-eval companion, i.e. a CTTS, but some HAeBes still seem to generate intrinsic X-ray emission (Hamaguchi et al. 2005; Skinner et al. 2004; Stelzer et al. 2006, 2009). There are two cases of HAeBes without any evidence of binarity and an existing X-ray grating spectrum: AB Aur (Telleschi et al. 2007c) and HD 163296 (Günther & Schmitt 2009; Swartz et al. 2005). Figure 8 shows the O VII triplets for those two HAeBes. The signal for AB Aur is weak, because it falls on the edge of the detector. Both stars seem to have strong *f* and weak *i* lines, for HD 163296 $f/i > 2.6$ on the 90% confidence level (Günther & Schmitt 2009). This means that the emission originates in a region of low density and, given the strong UV field on the surface of A-type stars,

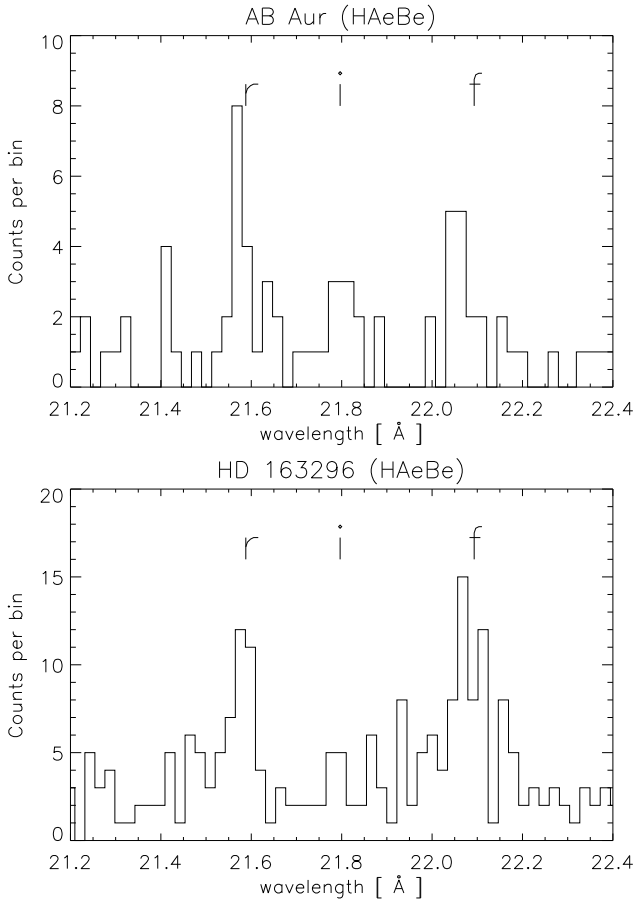


Fig. 8 O VII triplet for AB Aur (top) and HD 163296 (bottom) observed with *XMM-Newton*/RGS. *r*, *i* and *f* line are labeled.

this region is at a radius $R > 1.7 R_*$, i.e. at least $0.7 R_*$ above the surface. Otherwise, the UV photons would shift emission from the *f* to the *i* line. Given the low absorbing column density it is unlikely that the hot plasma resides in a region closer to the surface, that is somehow shielded from the stellar radiation field. HD 163296 is known to drive a powerful jet, just as the CTTS DG Tau, so a similar scenario, where the X-ray emission is caused by a shock in the jet, is possible. In fact, one knot in the jet of HD 163296 might itself be an X-ray source (Swartz et al. 2005). In addition to this soft component, HAeBes also show surprisingly hot emission with fitted temperatures around 30 MK. This cannot be caused by accretion and is a clear signature of magnetic activity. HAeBes are not expected to drive solar-like dynamos, but they might operate turbulent dynamos in the atmosphere or retain the primordial magnetic field of the interstellar cloud. If the field lines are frozen-in the field strength increases by many orders of magnitude during the collapse to the proto-star. Giardino et al. (2004) observed a large flare in V892 Tau, a system of a HAeBe with a companion. The system is not resolved but they could tentatively identify the flare with the HAeBe star. This fits the picture of a magnetically heated corona.

The absence of high-density emission and the minimum distance between O VII emission and the stellar surface shows that accretion does not contribute to the X-ray emission from HAeBes. Likely, the accretion process differs from CTTS, because the magnetic field is not strong enough to disrupt the disk at the co-rotation radius and to support magnetically funneled accretion. The mass may reach the star in the equatorial plane and form some kind of a boundary layer.

4 Summary

This article summarizes the results of high-resolution X-ray spectroscopy of young stars in the mass range of CTTS and HAeBes.

For two *Chandra* observations I could deblend the Mg XI triplet from the Ne Lyman series. It turns out that the Ne blend is weak, despite the enhanced Ne abundance.

At least three different processes contribute to the X-ray emission from CTTS, their importance varies between individual objects. First, there is a solar-like corona, second, the post-shock zone of the accretion shock cools radiating in X-rays and other wavelengths and, third, internal shocks in jets can heat matter to X-ray emitting temperatures. This is studied for the individual sources with the best spectra, but there is no reason why these results should not apply to CTTS as a class. The combined models explain the observed line ratios in the He-like triplets of O VII and Ne IX very well.

The mass accretion rate required to power the X-ray emission is typically lower than values estimated from other wavelengths. This might be due to inhomogeneous spots, partial absorption or accretion streams, which impact at velocities significantly below the free-fall speed.

The mass flux in the X-ray component of the DG Tau jets is also 10^{-3} of the total mass loss rate. This is fully compatible with optical observations, that show only the innermost jet component to be sufficiently fast (400 to 500 km s $^{-1}$) to heat the gas in shocks to X-ray emitting temperatures. For an electron density $> 10^5$ cm $^{-3}$ all dimensions of the shock cooling zone are only a few λ_0 , so even in optical observations this cannot be resolved.

The circumstellar environment of some CTTS differs markedly from the interstellar gas-to-dust ratio. This can be explained, if the outflows of those CTTS are dust-depleted.

Last, the X-ray emission from HAeBes is likely intrinsic and not due to an unresolved companion. It can thus be established that HAeBes have a hot emission component similar to a solar-like corona. The line ratio in the O VII He-like triplet rules out an accretion shock origin for the soft emission. Likely, a large fraction of the soft component is produced in the jet similar to DG Tau.

Acknowledgements. I thank the Astronomische Gesellschaft for awarding me the newly established Promotionspreis in 2010. The work, which is summarized in this article, would not have been possible without the help and advice of my colleagues at the Hamburger Sternwarte and especially my thesis adviser Prof. J. H. M. M.

Schmitt. Jan-Uwe Ness helped a lot in the CORA fits to the Mg triplet. H. M. G. acknowledges financial support from Chandra grant GO6-7017X and from the Faculty of the European Space Astronomy Centre. This research made use of the Chandra Transmission Grating Catalog and archive (<http://tgcat.mit.edu>).

References

- Alcala, J. M., Krautter, J., Schmitt, J. H. M. M., et al. 1995, *A&AS*, 114, 109
- Alcala, J. M., Terranegra, L., Wichmann, R., et al. 1996, *A&AS*, 119, 7
- Alencar, S. H. P. & Basri, G. 2000, *AJ*, 119, 1881
- Anderson, J. M., Li, Z.-Y., Krasnopolsky, R., & Blandford, R. D. 2005, *ApJ*, 630, 945
- Ardila, D. R., Basri, G., Walter, F. M., Valenti, J. A., & Johns-Krull, C. M. 2002a, *ApJ*, 566, 1100
- Ardila, D. R., Basri, G., Walter, F. M., Valenti, J. A., & Johns-Krull, C. M. 2002b, *ApJ*, 567, 1013
- Argiroffi, C., Maggio, A., & Peres, G. 2007, *A&A*, 465, L5
- Argiroffi, C., Maggio, A., Peres, G., et al. 2009, *A&A*, 507, 939
- Argiroffi, C., Maggio, A., Peres, G., Stelzer, B., & Neuhäuser, R. 2005, *A&A*, 439, 1149
- Arnaud, K. A. 1996, in *ASP Conf. Ser. 101: Astronomical Data Analysis Software and Systems V*, 17–+
- Bacciotti, F., Mundt, R., Ray, T. P., et al. 2000, *ApJ*, 537, L49
- Bally, J., Feigelson, E., & Reipurth, B. 2003, *ApJ*, 584, 843
- Bally, J., Reipurth, B., & Davis, C. J. 2007, in *Protostars and Planets V*, ed. B. Reipurth, D. Jewitt, & K. Keil, 215–230
- Balucinska-Church, M. & McCammon, D. 1992, *ApJ*, 400, 699
- Beristain, G., Edwards, S., & Kwan, J. 2001, *ApJ*, 551, 1037
- Bertout, C., Basri, G., & Bouvier, J. 1988, *ApJ*, 330, 350
- Blandford, R. D. & Payne, D. G. 1982, *MNRAS*, 199, 883
- Brickhouse, N. S., Cranmer, S. R., Dupree, A. K., Luna, G. J. M., & Wolk, S. 2010, *ApJ*, 710, 1835
- Calvet, N. & Gullbring, E. 1998, *ApJ*, 509, 802
- Cardelli, J. A., Clayton, G. C., & Mathis, J. S. 1989, *ApJ*, 345, 245
- Coffey, D., Bacciotti, F., Woitas, J., Ray, T. P., & Eisloffel, J. 2004, *ApJ*, 604, 758
- Curran, R. L., Argiroffi, C., Sacco, G. G., et al. 2010, *ArXiv e-prints*
- Dere, K. P., Landi, E., Mason, H. E., Fossi, B. C. M., & Young, P. R. 1998, in *ASP Conf. Ser. 143: The Scientific Impact of the Goddard High Resolution Spectrograph*, 390–+
- Donati, J.-F., Jardine, M. M., Gregory, S. G., et al. 2007, *MNRAS*, 380, 1297
- Donati, J.-F., Jardine, M. M., Gregory, S. G., et al. 2008, *MNRAS*, 386, 1234
- Drake, J. J. 2005, in *13th Cambridge Workshop on Cool Stars, Stellar Systems and the Sun*, 519–523
- Drake, J. J., Ratzlaff, P. W., Laming, J. M., & Raymond, J. 2009, *ApJ*, 703, 1224
- Dupree, A. K., Brickhouse, N. S., Smith, G. H., & Strader, J. 2005a, *ApJ*, 625, L131
- Dupree, A. K., Lobel, A., Young, P. R., et al. 2005b, *ApJ*, 622, 629
- Edwards, S., Fischer, W., Hillenbrand, L., & Kwan, J. 2006, *ApJ*, 646, 319
- Eisner, J. A., Chiang, E. I., & Hillenbrand, L. A. 2006, *ApJ*, 637, L133
- Fang, M., van Boekel, R., Wang, W., et al. 2009, *A&A*, 504, 461
- Favata, F., Bonito, R., Micela, G., et al. 2006, *A&A*, 450, L17
- Favata, F., Fridlund, C. V. M., Micela, G., Sciortino, S., & Kaas, A. A. 2002, *A&A*, 386, 204
- Feigelson, E. D. & Decampli, W. M. 1981, *ApJ*, 243, L89
- Feigelson, E. D. & Montmerle, T. 1999, *ARA&A*, 37, 363
- Fruscione, A., McDowell, J. C., Allen, G. E., et al. 2006, in *Society of Photo-Optical Instrumentation Engineers (SPIE) Conference Series*, Vol. 6270, Society of Photo-Optical Instrumentation Engineers (SPIE) Conference Series
- Gabriel, A. H. & Jordan, C. 1969, *MNRAS*, 145, 241
- Gabriel, C., Denby, M., Fyfe, D. J., et al. 2004, in *Astronomical Society of the Pacific Conference Series*, Vol. 314, *Astronomical Data Analysis Software and Systems (ADASS) XIII*, ed. F. Ochsenbein, M. G. Allen, & D. Egret, 759–+
- Getman, K. V., Feigelson, E. D., Broos, P. S., Micela, G., & Garmire, G. P. 2008a, *ApJ*, 688, 418
- Getman, K. V., Feigelson, E. D., Micela, G., et al. 2008b, *ApJ*, 688, 437
- Getman, K. V., Flaccomio, E., Broos, P. S., et al. 2005, *ApJS*, 160, 319
- Giardino, G., Favata, F., Micela, G., & Reale, F. 2004, *A&A*, 413, 669
- Grevesse, N. & Sauval, A. J. 1998, *Space Science Reviews*, 85, 161
- Güdel, M. & Nazé, Y. 2009, *A&A Rev.*, 17, 309
- Güdel, M., Skinner, S. L., Briggs, K. R., et al. 2005, *ApJ*, 626, L53
- Güdel, M., Skinner, S. L., Mel'Nikov, S. Y., et al. 2007, *A&A*, 468, 529
- Güdel, M. & Telleschi, A. 2007, *A&A*, 474, L25
- Gullbring, E., Calvet, N., Muzerolle, J., & Hartmann, L. 2000, *ApJ*, 544, 927
- Günther, H. M., Lewandowska, N., Hundertmark, M. P. G., et al. 2010, *A&A*, 518, A54+
- Günther, H. M., Liefke, C., Schmitt, J. H. M. M., Robrade, J., & Ness, J.-U. 2006, *A&A*, 459, L29
- Günther, H. M., Matt, S. P., & Li, Z.-Y. 2009, *A&A*, 493, 579
- Günther, H. M. & Schmitt, J. H. M. M. 2007, *Memorie della Società Astronomica Italiana*, 78, 359
- Günther, H. M. & Schmitt, J. H. M. M. 2008, *A&A*, 481, 735
- Günther, H. M. & Schmitt, J. H. M. M. 2009, *A&A*, 494, 1041
- Günther, H. M., Schmitt, J. H. M. M., Robrade, J., & Liefke, C. 2007, *A&A*, 466, 1111
- Hamaguchi, K., Yamauchi, S., & Koyama, K. 2005, *ApJ*, 618, 360
- Hartigan, P., Edwards, S., & Ghandour, L. 1995, *ApJ*, 452, 736
- Herczeg, G. J., Linsky, J. L., Valenti, J. A., Johns-Krull, C. M., & Wood, B. E. 2002, *ApJ*, 572, 310
- Herczeg, G. J., Linsky, J. L., Walter, F. M., Gahm, G. F., & Johns-Krull, C. M. 2006, *ApJS*, 165, 256
- Herczeg, G. J., Walter, F. M., Linsky, J. L., et al. 2005, *AJ*, 129, 2777
- Huenemoerder, D. P., Kastner, J. H., Testa, P., Schulz, N. S., & Weintraub, D. A. 2007, *ApJ*, 671, 592
- Johns-Krull, C. M. & Herczeg, G. J. 2007, *ApJ*, 655, 345
- Kastner, J. H., Huenemoerder, D. P., Schulz, N. S., et al. 2004, *ApJ*, 605, L49
- Kastner, J. H., Huenemoerder, D. P., Schulz, N. S., Canizares, C. R., & Weintraub, D. A. 2002, *ApJ*, 567, 434
- Koenigl, A. 1991, *ApJ*, 370, L39
- Koldoba, A. V., Ustyugova, G. V., Romanova, M. M., & Lovelace,

- R. V. E. 2008, MNRAS , 388, 357
- Kwan, J. & Tademaru, E. 1988, ApJ , 332, L41
- Lamzin, S. A. 1998, Astronomy Reports, 42, 322
- Lamzin, S. A., Kravtsova, A. S., Romanova, M. M., & Batalha, C. 2004, Astronomy Letters, 30, 413
- Landi, E., Del Zanna, G., Young, P. R., et al. 2006, ApJS , 162, 261
- Lavalley, C., Cabrit, S., Dougados, C., Ferruit, P., & Bacon, R. 1997, A&A , 327, 671
- Lavalley-Fouquet, C., Cabrit, S., & Dougados, C. 2000, A&A , 356, L41
- Long, M., Romanova, M. M., & Lovelace, R. V. E. 2007, MNRAS , 374, 436
- Matt, S. & Pudritz, R. E. 2005, ApJ , 632, L135
- Muzerolle, J., Calvet, N., & Hartmann, L. 1998a, ApJ , 492, 743
- Muzerolle, J., Calvet, N., Hartmann, L., & D'Alessio, P. 2003, ApJ , 597, L149
- Muzerolle, J., Hartmann, L., & Calvet, N. 1998b, AJ , 116, 2965
- Ness, J.-U., Güdel, M., Schmitt, J. H. M. M., Audard, M., & Telleschi, A. 2004, A&A , 427, 667
- Ness, J.-U. & Wichmann, R. 2002, Astronomische Nachrichten, 323, 129
- Neuhäuser, R., Sterzik, M. F., Schmitt, J. H. M. M., Wichmann, R., & Krautter, J. 1995, A&A , 297, 391
- Orlando, S., Sacco, G. G., Argiroffi, C., et al. 2010, A&A , 510, A71+
- Padgett, D. L., Cieza, L., Stapelfeldt, K. R., et al. 2006, ApJ , 645, 1283
- Porquet, D., Mewe, R., Dubau, J., Raassen, A. J. J., & Kaastra, J. S. 2001, A&A , 376, 1113
- Pravdo, S. H., Feigelson, E. D., Garmire, G., et al. 2001, Nature , 413, 708
- Preibisch, T., Kim, Y.-C., Favata, F., et al. 2005, ApJS , 160, 401
- Pyo, T.-S., Kobayashi, N., Hayashi, M., et al. 2003, ApJ , 590, 340
- Raassen, A. J. J. 2009, A&A , 505, 755
- Redfield, S., Linsky, J. L., Ake, T. B., et al. 2002, ApJ , 581, 626
- Robrade, J. & Schmitt, J. H. M. M. 2007, A&A , 473, 229
- Rodriguez, L. F. 1995, in Revista Mexicana de Astronomia y Astrofisica Conference Series, ed. S. Lizano & J. M. Torrelles, 1—
- Romanova, M. M., Ustyugova, G. V., Koldoba, A. V., & Lovelace, R. V. E. 2004, ApJ , 610, 920
- Sacco, G. G., Argiroffi, C., Orlando, S., et al. 2008, A&A , 491, L17
- Schmitt, J. H. M. M., Robrade, J., Ness, J.-U., Favata, F., & Stelzer, B. 2005, A&A , 432, L35
- Shu, F., Najita, J., Ostriker, E., et al. 1994, ApJ , 429, 781
- Skinner, S. L., Güdel, M., Audard, M., & Smith, K. 2004, ApJ , 614, 221
- Stelzer, B., Flaccomio, E., Briggs, K., et al. 2007, A&A , 468, 463
- Stelzer, B., Micela, G., Hamaguchi, K., & Schmitt, J. H. M. M. 2006, A&A , 457, 223
- Stelzer, B. & Neuhäuser, R. 2001, A&A , 377, 538
- Stelzer, B., Robrade, J., Schmitt, J. H. M. M., & Bouvier, J. 2009, A&A , 493, 1109
- Stelzer, B. & Schmitt, J. H. M. M. 2004, A&A , 418, 687
- Strassmeier, K. G., Rice, J. B., Ritter, A., et al. 2005, A&A , 440, 1105
- Swartz, D. A., Drake, J. J., Elsner, R. F., et al. 2005, ApJ , 628, 811
- Takami, M., Chrysostomou, A., Ray, T. P., et al. 2004, A&A , 416, 213
- Telleschi, A., Güdel, M., Briggs, K. R., Audard, M., & Palla, F. 2007a, A&A , 468, 425
- Telleschi, A., Güdel, M., Briggs, K. R., Audard, M., & Scelsi, L. 2007b, A&A , 468, 443
- Telleschi, A., Güdel, M., Briggs, K. R., et al. 2007c, A&A , 468, 541
- Testa, P., Drake, J. J., & Peres, G. 2004, ApJ , 617, 508
- Uchida, Y. & Shibata, K. 1984, PASJ , 36, 105
- Unruh, Y. C., Collier Cameron, A., & Guenther, E. 1998, MNRAS , 295, 781
- Vuong, M. H., Montmerle, T., Grosso, N., et al. 2003, A&A , 408, 581
- Zinnecker, H. & Preibisch, T. 1994, A&A , 292, 152